
Effects of Textures on Hydrogen Diffusion in Nickel

Introduction

The transition metal–hydrogen systems have been intensively researched for many years because of the various applications of these systems. A large hydrogen solubility in some transition metals allows their use for safe and high-capacity hydrogen storage.^{1,2} At the other end of the spectrum, hydrogen ingress at low concentrations can induce mechanical degradation of nickel and nickel alloys and compromise the intended application of the metal.^{1,3} An understanding of hydrogen adsorption/desorption characteristics on, and hydrogen mobility in, the metals is needed to predict the hydrogen impact on the metal systems.

Both deuterium and tritium are used as fuel for inertial confinement fusion (ICF) energy. In ICF applications, both adsorption on surfaces and permeation through metals are of importance. Hydrogen adsorption and desorption processes intimately control the degree to which surfaces become contaminated and subsequently the extent to which these surfaces can be decontaminated. In general, the smaller the adsorption rate, the shorter the residence time on a surface, and the simpler the structure of the oxide on a surface, the less susceptible that surface is to tritium contamination for a given set of exposure conditions. Contamination can proceed by simple condensation on a surface followed by absorption into the subsurface structure and by beta-activated radical surface reactions that capture mobile tritium atoms on surfaces into more tightly bound tritium-bearing complexes that are difficult to remove.

Surface tritium can also be absorbed into the metal and permeate to the opposite side, from where it can escape the process loop or contaminate a coolant circuit. For example, a nickel-alloy vessel with 1/32-in.-thick walls filled with tritium gas at 1 atm and room temperature will permeate 0.3 pCi/s/cm² in steady state, a tolerable release rate in part because the time to attain steady state is 6.3 years. At 300°C, however, this container will reach steady-state permeation within 1.6 h and release tritium at 0.8 μCi/s/cm². Such releases are unacceptably high and require intervention to preclude unacceptable releases to the environment or accumulation in cooling cir-

cuits. Permeation-resistant barriers, engineered composites, and low-absorption-coated, textured surfaces can offer relief from these emissions.

Hydrogen molecules dissociate on metal surfaces, dissolve atomically into the substructure, and interact with the microstructure of the metals. The interaction depends not only on the hydrogen concentration in the bulk but also on the prevalent microstructure; i.e., the mixture of crystal defects, grain boundaries, grain size, grain orientation, and phase composition present within the metal matrix. The density and blend of these features depends on the manufacturing and operating history of the metal.

For example, electrodeposition is the preferred approach to fabricate nickel membranes in industry. The texture of the nickel membranes can be controlled by the deposition parameters. Since hydrogen permeation in single-crystal metals is anisotropic, textured polycrystalline metals may exhibit different permeation properties for different textures. While an earlier study⁴ has shown that texture can influence hydrogen adsorption and diffusion in metals, to date there has been no systematic investigation of the effect of textures on hydrogen permeation through nickel. In this article, the relationship between hydrogen permeation and grain orientation in nickel membranes is studied. To this end, the following section outlines the experimental procedures used to prepare and characterize the nickel membranes and to measure the permeability of the membrane. Subsequent sections describe the details of the microstructure and its influence on permeation.

Experimental Procedure

Nickel membranes were electroplated in a Watt's bath at 50°C. The electrolyte comprised 300 g/l of NiSO₄ • 6H₂O, 35 g/l of NiCl₂ • 6H₂O, and 35 g/l of H₃CO₃ to make a pH-3 liquid. The electroplating current density was controlled galvanostatically between 0.1 to 0.8 A/cm². The anode was pure nickel. A titanium cathode substrate was chosen to support the nickel film during deposition because the nickel membranes could be easily peeled off. The substrate surface

was mechanically polished to minimize imprinting the substrate grain structure on the growing nickel film. Additionally, film thickness usually exceeded $50\ \mu\text{m}$ to further minimize imprinting the substrate orientation on the film's texture in preference for that favored by the electrodeposition parameters. The nickel deposits were then removed from the substrates to measure their grain orientation without any interference from the substrate. The permeability of these membranes were subsequently studied in an electrochemical cell.

The membrane surface texture was measured with a Siemens x-ray diffractometer outfitted with a molybdenum target. Maps of the orientation of the (100), (110), and (111) directions were measured in 5° polar and radial steps up to a maximum tilt of 80° . Orientation distribution functions (ODF) were calculated from these maps, also known as pole figures, according to the procedure described by Bunge⁵ with the aid of the software TexTool 3.0.

Hydrogen permeation was measured electrochemically with the aid of two cells separated by the nickel membrane of interest using the configuration shown in the Fig. 91.32. Hydrogen was injected into the membrane on the upstream side at a fixed rate, and the extraction rate was measured on the downstream side.

The electrolyte in both cells was 0.1 N NaOH to yield a pH 13 solution. On the exit (anode) side, a separate Ni/NiO electrode served as a saturated calomel electrode to maintain the membrane at a constant potential of 0.3 V relative to the anode. Prior to any measurements, both compartments were deoxygenated by bubbling nitrogen gas through the solutions. The measurements were carried out at 22°C . Before charging the membrane, an anodic potential 0.3 V was applied for 24 h to extract any residual hydrogen from the membrane and to reduce the background permeation current density. A graphite

cathode on the entry side was polarized galvanostatically to ensure that the singly charged ionic hydrogen flux impinging on the upstream surface was constant and fixed at a current density of $0.1\ \text{mA}/\text{cm}^2$. At this current density, the hydrogen flux reaching the membrane is 6×10^{14} particles/s- cm^2 . Permeant hydrogen is collected downstream of the membrane as the anodic current flows between the membrane and the anode. Sometime after the initiation of a cathodic current, an anodic current appears downstream and grows in strength to a maximum value. At this time, the hydrogen concentration gradient across the membrane thickness is linear, being highest at the entry side and nearly zero at the exit side. The time integral of the permeation current becomes constant once the linear concentration gradient is established within the membrane. Extrapolating the straight portion of the time-integrated curve back to the time axis yields a unique value known as the lag time (t_L). This time is related to the hydrogen diffusion coefficient (D) for the material⁶ by the relation

$$t_L = \frac{x^2}{2D}, \quad (1)$$

where x is the membrane thickness.

The concentration of adsorbed hydrogen on the upstream surface reflects the dynamic equilibrium between particles arriving from the electrolyte and particles disappearing into the metal. If the arrival flux rate far exceeds the absorption flux rate, hydrogen bubbles form on the upstream surface. Hydrogen transport through the metal is the rate-limiting step. If the absorption rate exceeds the arrival rate, the permeant flux is limited by the hydrogen arrival rate at the surface rather than by the adsorption rate into the metal. In this work, hydrogen transport through the metal is the rate-limiting step. In this case, steady-state permeation is described by Fick's First Law, and the concentration of absorbed hydrogen on the input

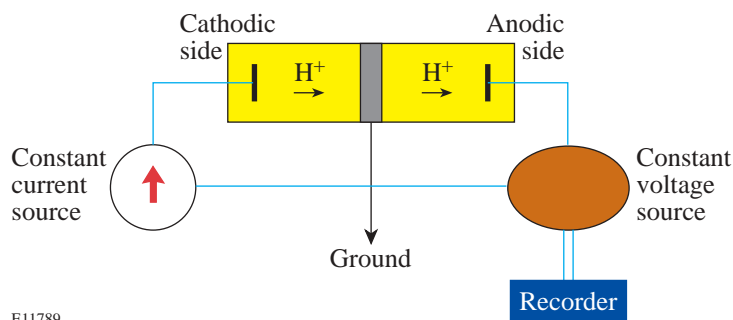


Figure 91.32
Schematic layout of the electrolytic permeation facility.

surface, C_0 , is uniquely related to the steady-state anodic current density I_{ss} by the relation

$$C_0 = \frac{I_{ss}x}{FD}, \quad (2)$$

where F is the Faraday constant (= 96,485 Coul/g-atm).

Results and Discussion

1. Microstructure and Texture

The microstructure across the cross section of each nickel deposit comprised three distinct zones. Grains in the vicinity of the film–substrate interface were equiaxed and fine. Immediately above this layer, the structure began to change from equiaxed grains to columnar grains. Beyond that and for the remainder of the film up to the nickel–air interface, the grains were columnar and orientated perpendicular to the substrate for most electroplating conditions.

The orientation of grains, i.e., the texture of the surface, was measured by Bragg diffraction to generate the ODF's. Figure 91.33 illustrates the ODF of the titanium substrate used in this work. This ODF is typical of a cold-rolled titanium plate.⁷ A typical ODF for a nickel membrane electrodeposited for the present work is presented in Fig. 91.34. Inspection of these two distribution functions indicates that there has been no textural imprinting by the substrate on the nickel deposit. The nickel texture has been determined solely by the deposition parameters.

Either (100) or (110) fiber textures can be obtained by changing the deposition conditions. At low current density, the (100) fiber texture is preferred. At high current density, the (110) fiber texture dominates. The (111) texture can be derived by annealing deposits with strong $\langle 100 \rangle$ texture at 800°C for 1 h.⁸

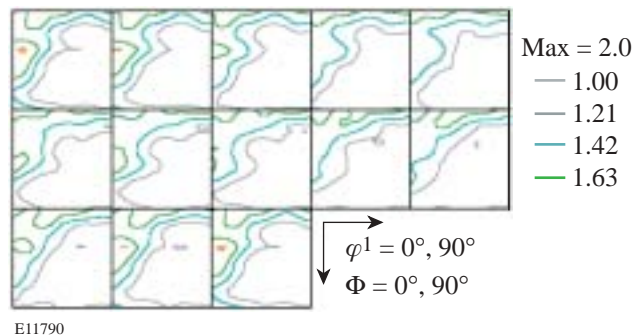


Figure 91.33
Orientation distribution function of the titanium substrate.

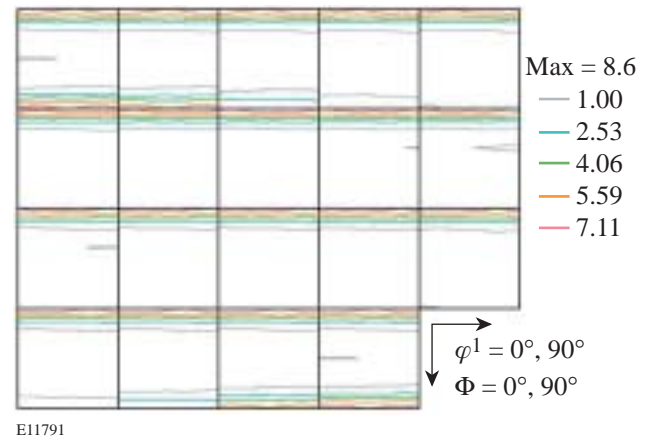


Figure 91.34
Orientation distribution function of nickel deposit.

2. Hydrogen Permeation and Analysis

The temporal behavior of hydrogen permeation through nickel with different textures is shown in Fig. 91.35. The permeation behavior for a nickel sample without any dominant texture has been included for reference. In all cases, the permeation current increases smoothly with increasing charging time to a maximum constant value. There are significant differences, however, among the textured and nontextured membranes. Hydrogen transport through (111) texture is faster than for any of the other textures. The time to attain steady-state permeation is longest in (110) texture nickel. Compared to the sample without any dominant texture, the response time for surfaces with a dominant texture is rapid.

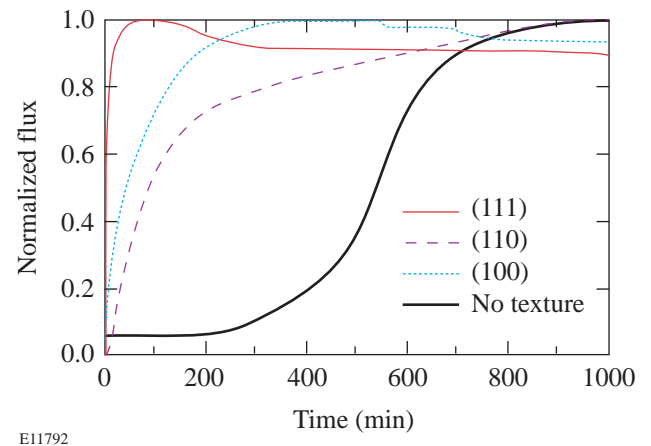


Figure 91.35
Temporal evolution of hydrogen permeation through nickel membrane with differing textures and for a sample without any dominant texture.

Hydrogen diffusivity and near-surface hydrogen concentration have been calculated using Eqs. (1) and (2) for the various nickel membranes and are listed in Table 91.III. Diffusion coefficients for (100) and (110) single-crystal samples have been provided for comparison. The coefficients are seen to increase as one moves toward more-open crystal structures, i.e., from (100) to (110) and then to (111) textured samples. The sample without any dominant texture exhibits the lowest diffusion coefficient of all the samples investigated. Diffusion coefficients for polycrystalline nickel membranes with dominant (100) and (110) textures are respectively higher than for (100) and (110) single-crystal membranes, but both exhibit the same trend when moving toward more-open structures, i.e., from (100) to (110) textures.

The near-surface concentration (C_0) of hydrogen in the sample without any dominant texture is the highest. The concentrations in (111) and (110) textured cases are the lowest of the samples studied and lie within experimental error of each other. This table suggests that the near-surface hydrogen concentration on the upstream side of the membrane is depleted by rapid transport through the membrane. The higher the diffusivity, the lower the subsurface hydrogen concentration.

Hydrogen permeation through a metal membrane in an electrochemical environment involves three steps: hydrogen atom absorption, diffusion across the membrane, and desorption. The molecular dissociation and the atomic association steps on the upstream and downstream sides of the membrane respectively that are normally associated with gas-phase hy-

drogen permeation are not present in this case because the hydrogen arrives and leaves the membrane as ions in the electrolyte. Hydrogen transport is characterized by three interaction energies: absorption, diffusion, and desorption. Typically adsorption and desorption energies are the same for polycrystalline metals without any dominant texture. The diffusion energy tends to be governed by bulk microstructural features, such as grain orientation, grain boundary density, and trap density. Both activation energies can influence the total hydrogen permeation flux and the temporal evolution of that flux.

Hydrogen adsorption energies differ for various crystal planes.¹²⁻¹⁴ These have been measured for the three low-index planes: (100), (110), and (111) of nickel.¹² The net adsorption energy of a surface can be estimated from weight-averaged linear combinations of adsorption energies on low-index planes and the preponderance of those planes on a specific surface. Typically, the results are displayed on an inverse pole figure to account for the distribution of the low-index planes in a selected direction in the specimen relative to the crystal axes. Crystals in face-centered cubic metals such as nickel possess higher degrees of symmetry, and the three low-index planes, (100), (110), and (111), are adequate to uniquely specify a surface orientation. Consequently only the unit stereographic triangle needs to be shown. Figure 91.36 displays the net surface adsorption energy dependence of hydrogen on nickel. This figure shows that the adsorption energy is highest for (100) and lowest for (111). Hydrogen is expected to adsorb more easily through (111) planes than either (100) or

Table 91.III: Hydrogen permeation data for nickel with different textural surfaces.

Membrane Surface Structure		D (10^{-9} cm ² /s) ±5%	C_0 (mmol/cm ³) ±10%
Polycrystalline Ni	No texture	2.6	0.38
	(100)	3.4	0.18
	(110)	6.5	0.12
	(111)	8.5	0.13
Single-Crystal Ni	(100)	0.56 (Ref. 9)	
		0.51 (Ref. 10)	
	(110)	0.62 (Ref. 11)	

(110) planes. As a consequence, hydrogen ingress and transport through nickel can be tailored by altering the surface orientation of crystals to favor or suppress the (111) plane.

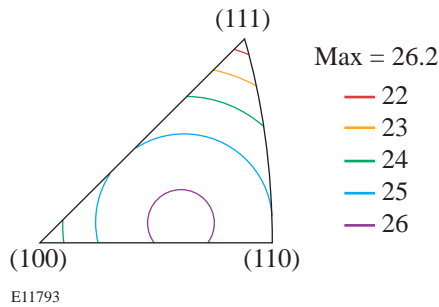


Figure 91.36
Hydrogen absorption energies for the three low-index planes in nickel.

Diffusivity can also be modulated by orientation.^{9–11} Table 91.III indicates that hydrogen transport is more rapid in single crystals via (110) than (100) orientations. Polycrystalline membranes are combinations of many single crystals with different orientations. Texturing a polycrystalline membrane provides a method for selecting a dominant orientation with the intent of enhancing or suppressing hydrogen adsorptions and subsequent transport. Hydrogen transport can be modulated by textural control in addition to the bulk microstructural features discussed earlier.

Conclusions

Nickel membranes with differing textures have been grown and analyzed. Deposition parameters that influence the texture during the growing process have been identified. These protocols were implemented to construct membranes for permeation experiments. Electrolytic permeation has been used to study the impact of texture on hydrogen permeation through nickel.

Four conclusions can be derived from this work: First, textured nickel films can be grown on titanium without textural imprinting from the substrate. Plating current density has a strong influence on texture forms of nickel deposits. At low current density, the (100) fiber texture is the dominant component; at high current density, the (110) fiber texture dominates. Annealing at 800°C for 1 h, (100) texture converts to (111) texture. Second, hydrogen permeation through nickel membranes depends on texture. Diffusion coefficients increase as one moves from (100) to (110) to (111) textured samples. The diffusion coefficient of a sample without a

dominant texture is smaller than for textured samples. Diffusion coefficients of polycrystalline textured membranes are higher than similar single-crystal membranes, but both sets of membranes exhibit similar trends in behavior. Third, adsorption energies for different orientations have been calculated by using the weight-averaged combinations of the absorption energies for the three basic planes in nickel: (100), (110), and (111). Absorption energies for different orientations are presented. Finally, hydrogen transport in the bulk is expected to depend on texture in addition to the microstructural features such as grain size, traps, and grain boundary density typically discussed in the literature.

ACKNOWLEDGMENT

This research was supported by the Natural Sciences and Engineering Research Council of Canada (NSERC) under CRD Grant # CRDPJ 207805-97 and Ontario Power Technologies.

REFERENCES

1. H. Wipf and R. G. Barnes, *Hydrogen in Metals III: Properties and Applications*, Topics in Applied Physics, Vol. 73 (Springer, Berlin, 1997).
2. K. Hong, *J. Alloys Compd.* **321**, 307 (2001).
3. R. M. Latanision and M. Kurkela, *Corrosion* **39**, 174 (1983).
4. Y. Cao, J. A. Spunar, and W. T. Shmayda, "Microstructure Control Factors of Hydrogen Diffusion Through Palladium and Pd-Ag Membranes," to be published in *Defect and Diffusion Forum*.
5. H.-J. Bunge, *Texture Analysis in Materials Science: Mathematical Methods* (Butterworths, London, 1982).
6. M. A. V. Devanathan and Z. Stachurski, *Proc. R. Soc. Lond. A, Math. Phys. Sci.* **270**, 90 (1962).
7. H. Inoue and N. Inakazu, in *Eighth International Conference on Textures of Materials (ICOTOM 8)*, edited by J. S. Kallend and G. Gottstein (The Metallurgical Society, Warrendale, PA, 1988), pp. 997–1004.
8. F. Czerwinski and J. A. Szpunar, *Corros. Sci.* **41**, 729 (1999).
9. A. M. Brass and A. Chanfreau, *Acta Mater.* **44**, 3823 (1996).
10. Y. Ebisuzaki, W. J. Kass, and M. O'Keefe, *J. Chem. Phys.* **46**, 1378 (1967).
11. A. M. Brass, A. Chanfreau, and J. Chene, in *Hydrogen Effects on Materials Behavior*, edited by N. R. Moody and A. W. Thompson (Minerals, Metals, and Materials Society, Warrendale, PA, 1990), pp. 19–31.
12. G. Kresse and J. Hafner, *Surf. Sci.* **459**, 287 (2000).
13. K. Christmann *et al.*, *J. Chem. Phys.* **70**, 4168 (1979).
14. G. Kresse, *Phys. Rev. B, Condens. Matter* **62**, 8295 (2000).

